

Mechanical properties of lattice truss structures made of a selective laser melted superalloy

Håkan Brodin^{1,2*} and Jonas Saarimäki²

¹ Siemens Industrial Turbomachinery AB, 612 31 Finspång, Sweden

² Linköping University, Department of Management and Engineering, Division of Engineering Materials, 581 83 Linköping, Sweden

* Corresponding author: hakan.brodin@liu.se

Abstract

Selective laser melting is a free-form manufacturing process, where components are built up layer by layer using metal powder. Complicated geometries can be manufactured and the exact dimensional tolerances allow direct manufacturing with a minimum of post-processing. Many materials are available in powder form today, e.g. aluminium, titanium, stainless steels, tool steels and superalloys. The current work is performed on a nickel based superalloy, conforming in principle to Hastelloy X.

Different lattice truss structures were manufactured with the selective laser melting process. In parallel, solid bars were produced with the same manufacturing process. Hollow rectangular tubes and composites of tubes with an interior of lattice truss structures were also manufactured. Hot rolled material of Hastelloy X was included for reference. Mechanical testing was performed in tension.

Mechanical testing shows that the selective laser produced material is highly anisotropic and that the material has many advantages compared to the traditionally manufactured Hastelloy X alloy. Tests also show that fracture is promoted along certain planes in the lattice truss structure

Keywords

free form fabrication, selective laser melting, superalloys, tensile testing, lattice

1. Introduction

Free form fabrication, rapid prototyping and 3D-printing are different designations for processes where material can be built to finished or near-finished shape without machining a block of material or casting material in a mould [1-3]. The processes were initially developed for very simple materials, such as thermoset plastics and plaster. Early-on laser was used to melt materials with a low melting point [4, 5], for instance brass. With some free-form manufacturing processes the material with a low melting point was mixed with a material of a high melting point (for instance brass and steel powders). A laser would be able to melt the brass, but steel would not melt, or only partially melt. This method for manufacturing materials would not be sufficient in cases where high stress or elevated temperature use will come into play. With improved process control and higher laser power, the range of materials was expanded. With a higher heat input, more difficult materials are possible to melt and it will be possible to create a microstructure with low amount of porosity and a material without internal defects such as solidification cracks or poor bonding [6].

Free-form fabrication of superalloys is gaining increased interest from the industry, since the available alloys range is growing. Today alloys for selective laser melting include aluminium, titanium, tool steel, stainless steel and heat resistant materials of cobalt- and nickel base [7-13]. In the case of melting of metal powders, the dominating manufacturing process is laser melting, often denoted selective laser melting (SLM) [6], direct laser metal sintering (DMLS) or LaserCusing. All of these names are trade marks for different companies manufacturing equipment for laser melting. The laser melting manufacturing process can briefly be described as a layer-by layer process, where powder is distributed on a powder bed, Figure 1. After powder distribution, the powder is melted

and a metal slice is formed on the powder bed.

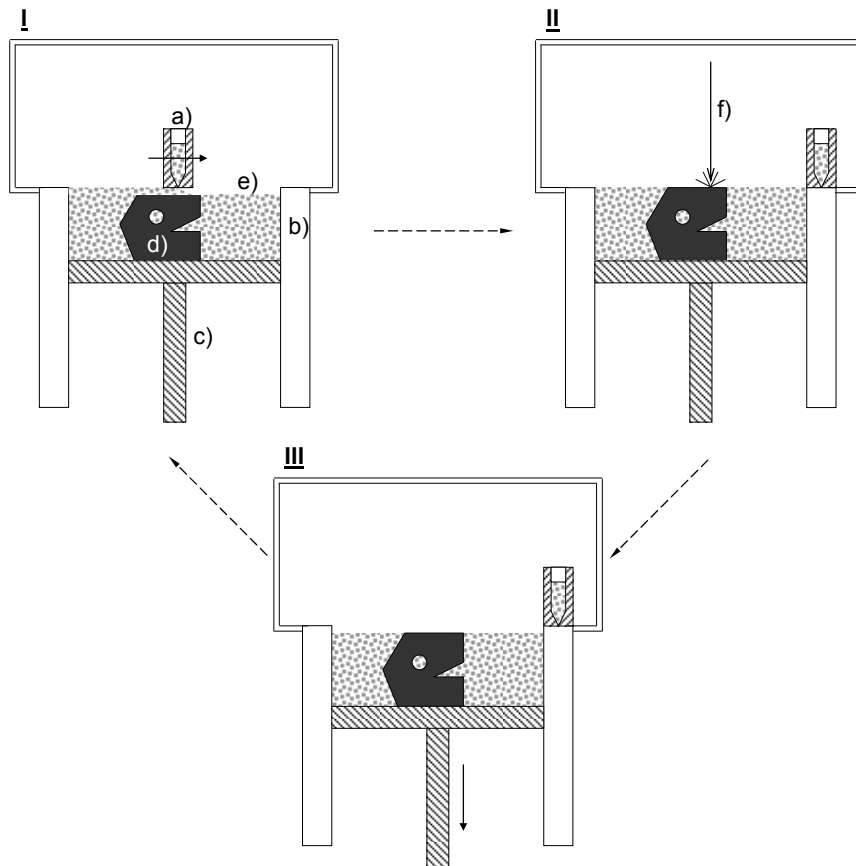


Figure 1. Schematic description of the SLM process. a) Powder is distributed on a powder bed, the build platform. b) The powder is melted by a laser beam and a slice of solid metal is formed. c) The powder bed is lowered and the process is repeated until a finished component is formed.

I: A powder distributor travels over the powder bed cavity contained by the build chamber walls b) and build plate c). Molten and solidified powder constitutes the component d) surrounded by unmolten powder e). II: A laser beam f) melts the powder layer and creates a new slice of solid material in the component d). III: A ram lowers the build platform c) and the process is repeated until a finished geometry is formed. After finalization, the remaining loose powder is removed and the component is cut off from the build platform.

2. Experimental details

2.1. Material

In the current work, material in principle conforming to AMS 5754 / UNS N06002 (i.e. Hastelloy X from Haynes International) has been used. In literature the material is sometimes identified as “Alloy X” when not available from the original supplier. The powder material is gas atomized and sieved to a fraction suitable for the SLM process, Figure 2. Solid test bars, hollow specimens and lattice truss structures with diamond geometry, Figure 3, were produced in an Eosint M270 DM machine. After manufacturing no heat treatment was adopted. In Table 1, the nominal composition of Hastelloy X is shown. The typical microstructure of the SLM material after manufacturing is shown below, Figure 4.

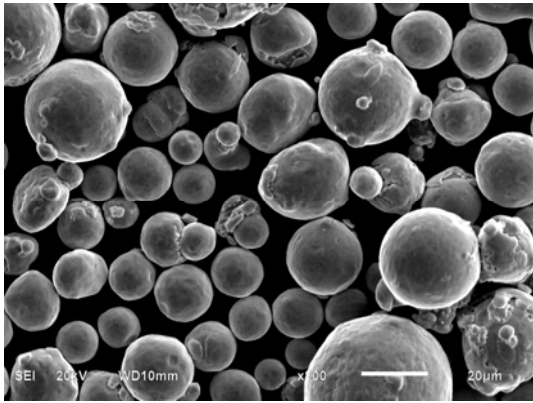


Figure 2. Morphology of the gas atomized powder used for SLM manufacturing in the current work.

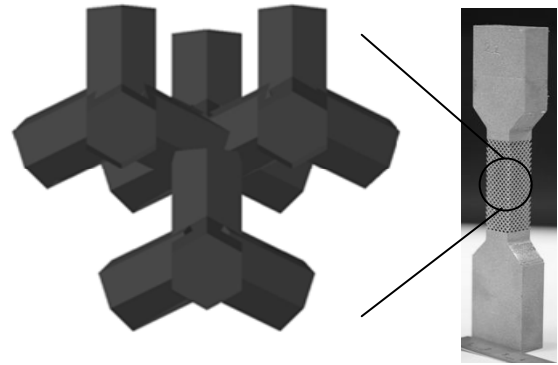


Figure 3. Least repetitive unit in diamond cell as used in the current work, here aligned in the 90° direction.

Table 1. Nominal composition of Hastelloy X as per standard for hot rolled material.

Ni	Cr	Fe	Mo	Co	Si	Mn	W
Bal.	22	18	9	1.5	<1	<1	0.6

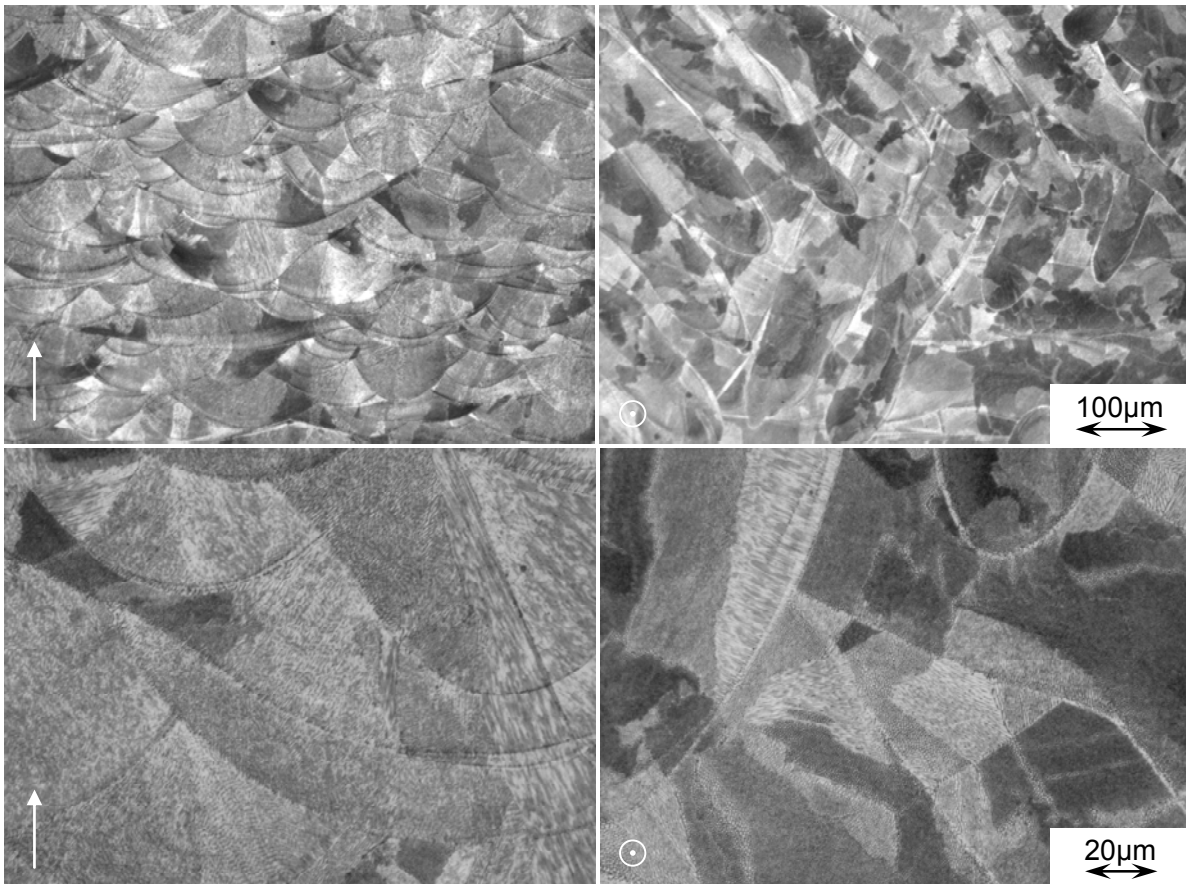


Figure 4. SLM bulk material in the as-manufactured condition. Top left (a) view parallel to build direction. Top right (b), view perpendicular to build direction. Bottom (c and d), close-up of weld-like structure after manufacturing. Build direction indicated by arrows.

2.2. Geometry

Different structures with and without lattices have been evaluated in the current work. Cross sections of the tubular shell, lattice and hybrid structures included are shown below, Figure 5. The lattice structure is designed to have a comparable density throughout the range of available dimensions. The measure d/l was kept constant throughout manufacturing of all test bars. As mentioned above, tensile testing was done using a “diamond” structure on the three different types of specimens a hollow tubular, an open lattice truss structure and a hybrid consisting of a tube containing a lattice truss structure as shown in Figure 5 containing the three different types of lattice truss structures. The structure sizes are called 2,2, 2,6 and 3,0 because of the dimensions that are calculated with the formula $w/s=v$ where w = cell size, s = lattice diameter and v is value that needs to be less than three for the structure to be manufactureable. The specimen sizes were chosen to be ($L \times W \times D$), $L \times 15 \times 15 \text{mm}$ and $L \times 13 \times 13 \text{mm}$ for the open lattice truss structure.

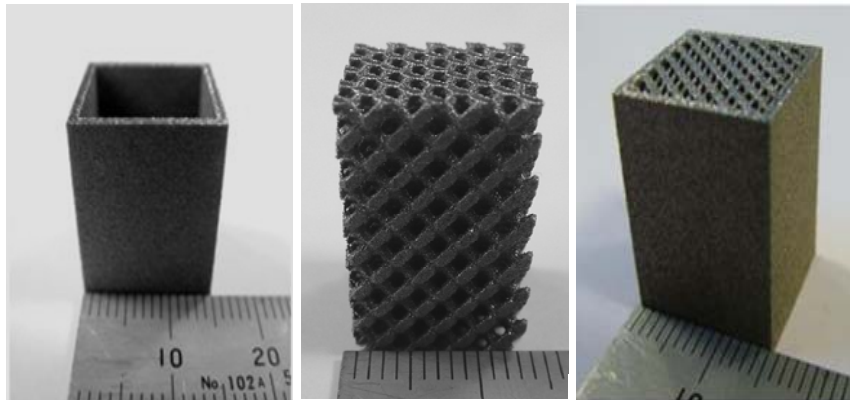


Figure 5. Cross-section of the three geometries for mechanical testing and evaluation of lattice truss structure testing: hollow shell (left), lattice truss structure (middle) and hybrid (right).

Tensile strength tests were done on laser sintered Alloy X at build angles of 0° and 90° . The results show that the mechanical properties vary considerably depending on the build angle. Build angle is defined with the specimen compared to the build platform and shown below, Figure 6.

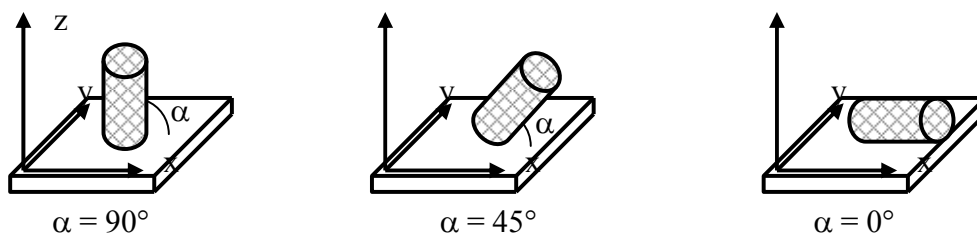


Figure 6. Definition of specimen build and loading direction relative to the build platform plane. A specimen “ 0° ” would be a specimen in any direction in the build plane and a specimen “ α° ” ($0^\circ < \alpha < 90^\circ$) would be a specimen built out of the build platform. An angle $\alpha = 90^\circ$ would indicate a specimen being built parallel to the SLM equipment build direction.

3. Results

3.1. Solid test bars

Tensile testing was conducted on solid material manufactured by selective laser melting and material produced by hot-rolling. Figure 7 shows typical tensile stress-strain data. The SLM material was tested in the as-manufactured state, whilst the hot-rolled material is tested in a solution heat treated material condition. In Figure 8 and Figure 9 more detailed tensile test results are shown for ambient and elevated temperature testing. Data are normalized to average values for hot-rolled Hastelloy X material.

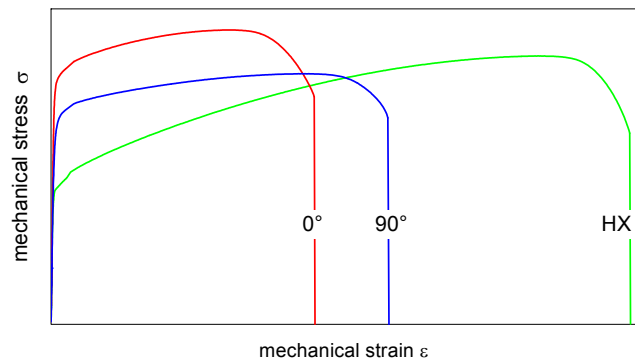


Figure 7. Generalized results from tensile testing of solid bars, stress-strain curves for standard Hastelloy X (HX), SLM Alloy X (0° and 90°).

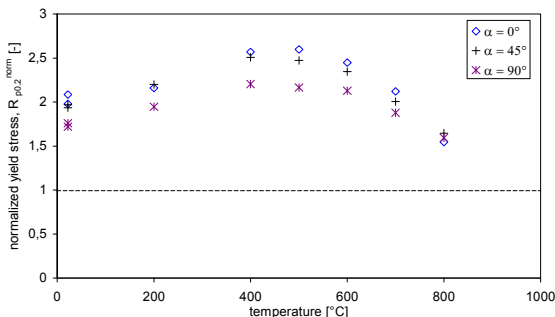


Figure 8. Normalized yield stress. Dashed line $R_{p0.2} = 1$ equals hot-rolled material.

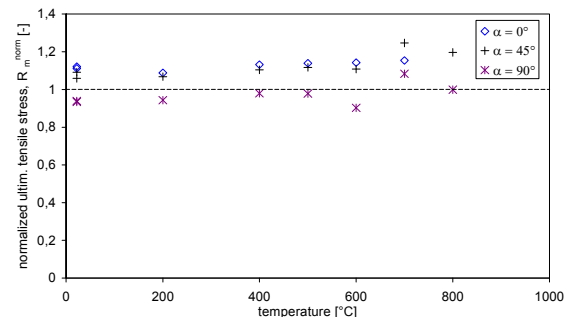


Figure 9. Normalized ultimate tensile stress. Dashed line $R_m = 1$ equals hot-rolled material.

Due to the weld-like manufacturing process, the material is highly anisotropic. This is clearly shown above in material data (Figure 7 to Figure 9) together with microstructural observations in Figure 4.

3.2. Lattice truss structures

Tensile testing has been performed on geometries as shown above, Figure 5. Results are presented and discussed below. From tensile tests, data for hollow, open lattice and hybrid structures are presented in Figure 10. The data set is a typical response from testing and represents all geometry variations 2.2 – 3.0 included in the test series.

The component stiffness can be calculated as the slope of the force-displacement curve for hollow,

open lattice and composite structures, since the tests here are performed on geometries where the hybrid specimen shell and the tubular specimens have identical shell measures. The open lattice truss structure was designed to fit inside the tube and, accordingly, the hybrid specimen interior hence matches the open truss structure.

In practical design work, the aim is often to use a light-weight material and data are often presented as a correlation between, for instance, density and stiffness. Plotting the material stiffness relative to measured density for open lattice, tubes and hybrid material yields Figure 11 below. For comparative purposes, the apparent density (the weight per unit volume of a material including internal cavities inherent in the material as tested) is used instead of density for a solid material.

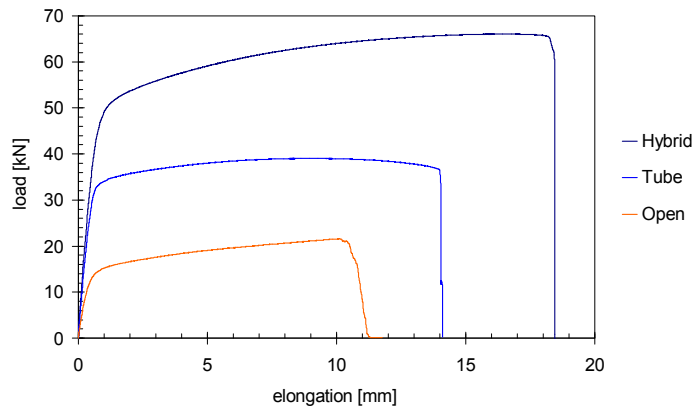


Figure 10. Tensile test results for the investigated geometries (tube, open lattice and hybrid test bar).

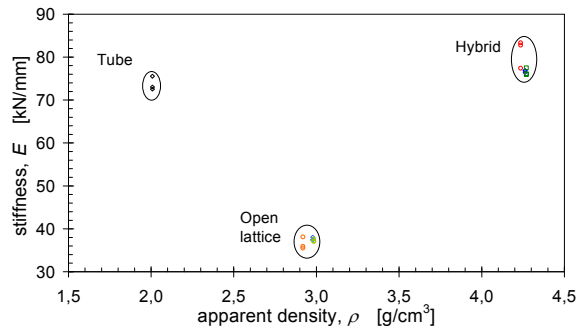


Figure 11. Design curves for measured stiffness E as a function of apparent density ρ .

Data have been further processed in order to compare stiffness, force at yield and peak force for the geometries in the test series. Comparisons are made of how an open truss structure and a tube interact in a hybrid material. Figure 12 shows a comparison between the measured behaviour (E , F_m and $F_{p0.2}$) of a hybrid test bar to the superpositioning of data for corresponding open lattice and tube specimen as shown below, Equation (1).

$$\begin{cases} E_s = E_t + E_{ol} \\ F_{p0.2, s} = F_{p0.2, t} + F_{p0.2, ol} \\ F_{m, s} = F_{m, t} + F_{m, ol} \end{cases} \quad (1)$$

where index “s” indicates superpositioned. “t” is tube and “ol” stands for open lattice. E is the stiffness (force/length) and $F_{p0.2}$ and F_m are force at yield and ultimate force. Due to the geometrical nature of the specimens, comparisons using these quantities are more convenient than quantities based on stress.

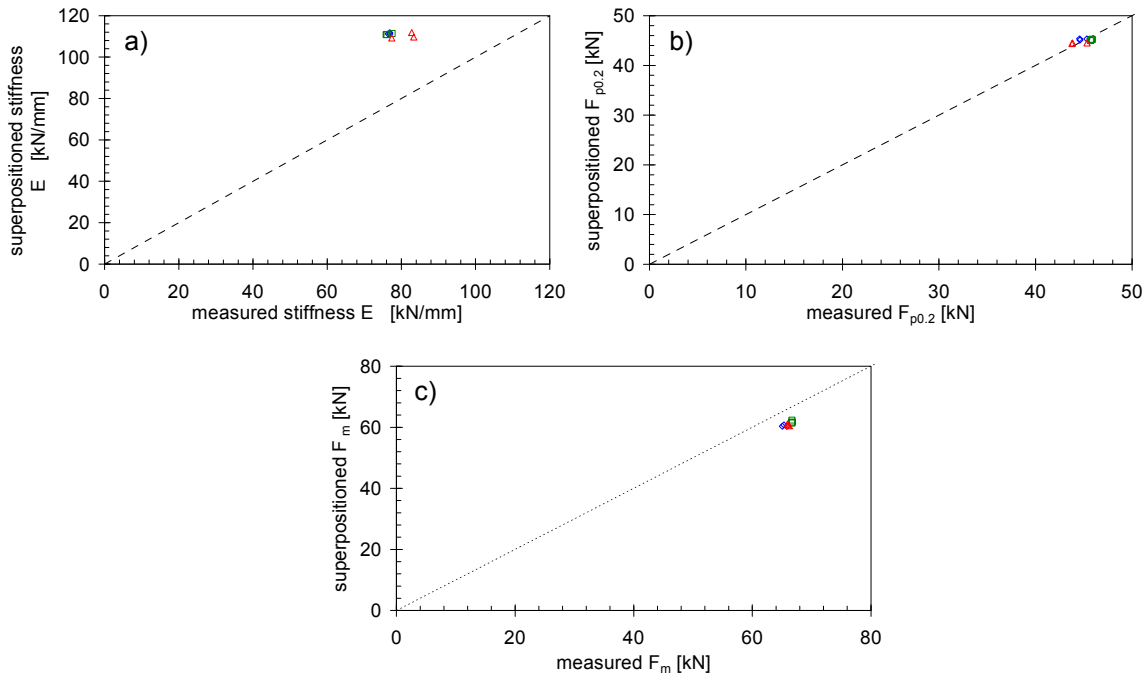


Figure 12. Comparison of superpositioned and measured stiffness E , load at yield $F_{p0.2}$ and maximum load before failure F_m for the hybrid geometry investigated in the current work.

3.3. Fracture surfaces

Fractographic observations from solid test bars and lattice trusses are shown below, Figure 13 to Figure 16. Figure 13 show the ductile fracture surface of an SLM manufactured solid test bar. In Figure 14 the failure of an open lattice truss structure is shown. In Figure 15 and Figure 16 bulk and surface regions of a lattice specimen can be viewed.

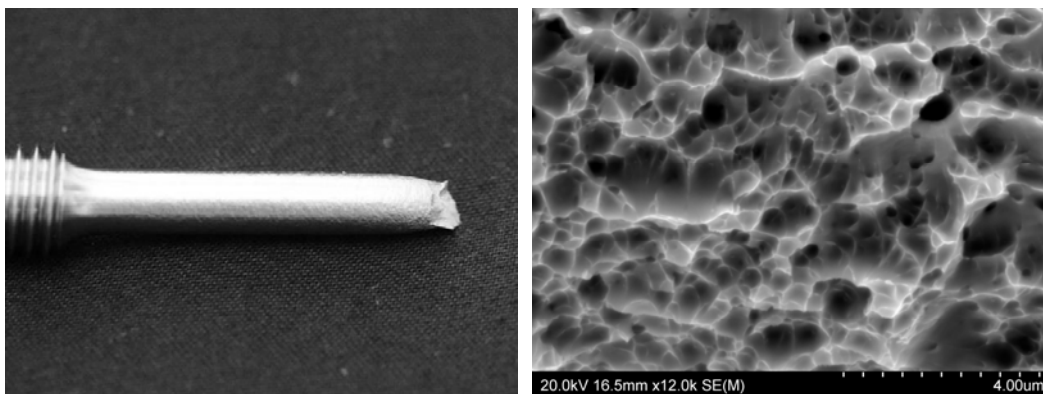


Figure 13. Typical cup and cone dimple fracture in solid as-manufactured alloy X manufactured by SLM (build and load direction perpendicular to build platform).

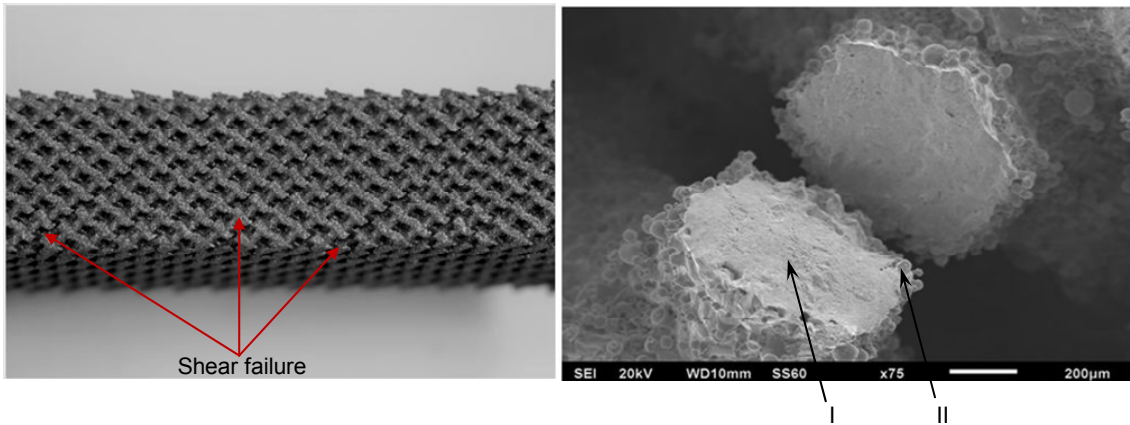


Figure 14. Typical shear damage of lattice struts due to axial tensile loading. Left: Shearing of the struts after tensile testing. Right: Shear fracture of a single strut after tensile testing. Note that the interior (I) and the exterior (II) exhibit differences in fracture appearance.

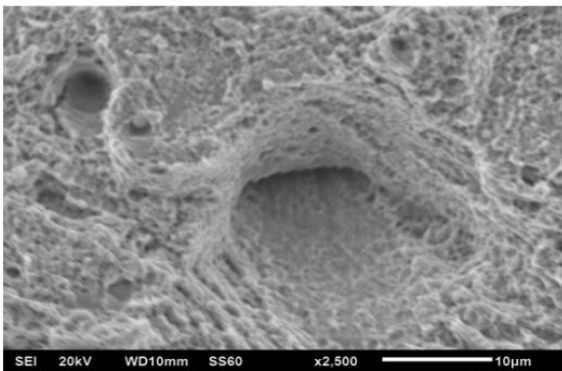


Figure 15. Strut failure of hybrid specimen.

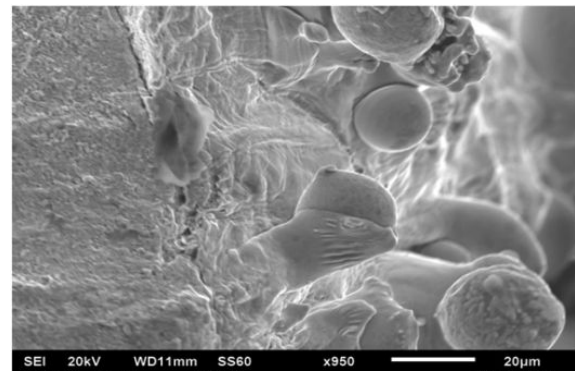


Figure 16. Fracture of as-manufactured surface. A skin of partly molten material is obvious.

4. Discussion

By comparison of data in Figure 11 and Figure 12 it is obvious that a superpositioning of stiffness for a tube and an open lattice structure does not equal the stiffness of a hybrid specimen. A conclusion must be that in tension the stiffness of a hybrid specimen is mainly influenced by the stiffness of the tube. I.e., for the tube the relation is according to Equation 2.

$$E_{hm} < E_t + E_{ol} \quad (2)$$

Regarding strength, in Figure 12 it is shown that for the geometry investigated here, the load is shared between the lattice structure and the tube so that the load applied to cause yield in the hybrid specimen equals the load applied to a tube and an open lattice as indicated by Equation 3.

$$F_{p0.2, hm} = F_{p0.2, t} + F_{p0.2, ol} \quad (3)$$

The same analysis for maximum load before failure yields that the maximum load in the hybrid specimen is slightly higher compared to the load in a tube and the open lattice superpositioned as described by Equation 4.

$$F_{m, hm} > F_{m, t} + F_{m, ol} \quad (4)$$

The reason for a stronger hybrid material can be attributed to change of constraint during loading. Figure 10 shows information on the material ductility. Not only does the hybrid material exhibit an increased strength compared to the tube plus open lattice but also a larger strain to failure (here plotted as elongation, which, in this case with equal initial lengths of the different geometries, yields comparable results).

The fractographic examination shows that the bulk SLM material is ductile with the expected cup and cone appearance and dimples on the tensile test specimen fracture surface. Open lattice truss structures and lattices in a hybrid specimen tend to fail due to a shear mechanism between struts along preferred planes. The typical fracture appearance is shown above in Figure 14. Tensile testing of components with as-manufactured surfaces reveals that the SLM material has a significant different fracture surface appearance in bulk and surface-near material. During manufacturing, SLM material will have a dense, completely remelted internal bulk. Externally, a thin layer of partly molten material will be present as observed in Figure 16.

5. Conclusions

The current paper shows how a selective laser melted material behaves in tensile testing. It is shown that the material is not as ductile as a normal hot-rolled material. However the material strength is good and the yield stress is superior to the hot-rolled material. Ultimate tensile strength is comparable between a selective laser melted material and the corresponding hot-rolled material. The selective laser melted material is highly anisotropic with respect to strength.

In light-weight designs, hybrid materials can easily be manufactured with the selective laser melting manufacturing method. It is shown that the yield strength of a hybrid material can be superpositioned by the yield strength of the individual shell and lattice structures. At failure the hybrid material will act stronger compared to the tubular shell and open lattice truss structure components in the hybrid part. The stiffness of the hybrid structure investigated here will mainly be influenced by the tubular shell.

6. References

- [1] Chu J., Engelbrecht S., Graf G., and Rosen D.W., 2010. "A comparison of synthesis methods for cellular structures with application to additive manufacturing". *Rapid Prototyping Journal*, 16, pp. 275-283.
- [2] Rosen D.W., 2007. "Computer-aided design for additive manufacturing of cellular structures". *Computer-Aided Design and Applications*, 4, pp. 585-594.
- [3] Marchelli G., Prabhakar R., Storti D., and Ganter M., 2011. "The guide to glass 3D printing: developments, methods, diagnostics and results". *Rapid Prototyping Journal*, 17(3), pp. 187 – 194.
- [4] Das S., Beama J.J., Wohler M., and Bourell D.L., 1998. "Direct laser freeform fabrication of high performance metal components". *Rapid Prototyping Journal*, 4(3), pp. 112 – 117.
- [5] Kruth J.P., Froyen L., Van Vaerenberg J., Mercelis P., Rombouts M., and Lauwers B., 2004. "Selective laser melting of iron-based powder". *Journal of Materials Processing Technology*, 149, pp. 616-622.

- [6] Agarwala M., Bourell D., Beaman J, Marcus H., and Barlow J., 1995. "Direct selective laser sintering of metals". *Rapid Prototyping Journal*, 1(1), pp. 26 – 36.
- [7] Abd-Elghany K., and Bourell D.L., 2012. "Property evaluation of 304L stainless steel fabricated by selective laser melting". *Rapid Prototyping Journal*, 18(5), pp. 420 – 428.
- [8] Li R., Liu J., Shi Y., Du M., and Xie Z., 2010. "316L Stainless Steel with Gradient Porosity Fabricated by Selective Laser Melting". *Journal of Materials Engineering and Performance*, 19(5), pp. 666-671.
- [9] Li R., Shi Y., Wang L., Liu J. and Wang Z., 2011. "Theory and technology of sintering, thermal and chemothermal treatment. The key metallurgical features of selective laser melting of stainless steel powder for building metallic part". *Powder Metallurgy and Metal Ceramics*, 50(3-4), pp. 141-151.
- [10] Buchbinder D., Schleifenbaum H., Heidrich S., Meiners W., and Bültmann J., 2011. "High Power Selective Laser Melting (HP SLM) of Aluminum Parts" *Physics Procedia*, 12, pp. 271–278.
- [11] Wang Z., Guan K., Gao M., Li X., Chen X., and Zeng X., 2012. "The microstructure and mechanical properties of deposited-In718 by selective laser melting". *Journal of Alloys and Compounds*, 513(5), pp. 518-523.
- [12] Vilaro T., Colin C., Bartout J.D., Nazé L., and Sennour M., 2012. "Microstructural and mechanical approaches of the selective laser melting process applied to a nickel-base superalloy" *Materials Science and Engineering A*, 534, pp. 446-451.
- [13] Wang F., 2012. "Mechanical property study on rapid additive layer manufacture Hastelloy® X alloy by selective laser melting technology". *International Journal of Advanced Manufacturing Technology*, 58, pp. 545-551.